Radio Jet Interactions with Massive Clouds

Z. Wang,[1] Paul J. Wiita and Jagbir S. Hooda[2]
Department of Physics and Astronomy, Georgia State University, Atlanta, GA 30303

ABSTRACT

Three-dimensional simulations of hydrodynamic jets are computed at rather high resolution using the Zeus-3D code. The parameters we employ are suitable for moderate to high power radio jets emerging through a galactic atmosphere or halo, and eventually crossing a tilted pressure matched interface with a hotter intracluster medium. Before they cross this interface, these simulations aim the jets so that they hit massive clouds within the galactic halo, with densities 10 or more times higher than the ambient atmospheric density, and 100's–1000's of times the jet density. Such clouds are set up with radii several times that of the jet, and could correspond to giant molecular cloud complexes or small cannibalized galaxies.

We find that while powerful jets eventually disperse the clouds, for off-center collisions, non-axisymmetric instabilities are induced in those jets. Those instabilities grow faster for lower Mach number jets, and can disrupt the jets substantially sooner than occurs for similar simulations of jets not hitting clouds. Such interactions could be related to some Compact Steep Spectrum source morphologies. Weak jets can be effectively halted or destroyed by reasonably massive clouds, and this type of interaction may have relevance for the paucity of extended radio jets in spiral galaxies. Slow, dense jets may be bent, yet remain stable for fairly extended times, and such interactions can be responsible for some of the wide-angle-tail and most of the "dog-leg" radio source morphologies.

Subject headings: galaxies: active — galaxies: jets — hydrodynamics — radio continuum

---

[1]current address: Department of Physics, Massachusetts Institute of Technology, Cambridge, MA

[2]current address: Institute of Paper Science & Technology, Atlanta, GA

1. Introduction

An extragalactic jet can interact powerfully with the environment along its path. One common morphological class of radio sources, the wide-angle tail (WAT) sources, may show both gradual and rather abrupt bends, with the deflection corresponding to a region of enhanced emissivity (e.g., O'Dea 1985; O'Donoghue Eilek, & Owen, 1993). One possible way to explain some of these structures would be for the jets to strike large dense clouds in the interstellar (ISM) or intracluster medium (ICM), so that the jet/cloud interactions produce deflections. However, numerical simulations have shown that strong gas motions in the intracluster medium, induced by galactic mergers, can produce many aspects of WAT structures (e.g., Loken et al. 1995). Still, the very abrupt bends seen in some powerful double sources, sometimes called "dog-leg" quasars (e.g., 3C 270.1, 3C 275.1, 4C 25.01; Stocke, Burns & Christiansen 1985) may be attributed to collisions between jets and massive clouds or smaller galaxies. Similar distorted structures were found to be moderately frequent in a survey by Hintzen, Ulvestad & Owen (1983).

Recent support for the concept of strong interactions has come from an investigation of the radio-optical alignment effect (e.g., McCarthy et al. 1987; Chambers, Miley & van Breugel 1987) by Best, Longair & Röttgering (1997) and Best et al. (1998). Using images taken by the Hubble Space Telescope and high-resolution radio observations, Best et al. (1997, 1998) found radio jets strongly correlated with the bright optical knots for 3C 34, 3C 324 and 3C 368. The object 3C 441 (Lacy et al. 1998) shows a similar structure. X-ray emission has been detected by Harris, Leighly & Leahy (1998) around a hot spot of the radio jet in 3C 390.3. These observations indicate that a jet may impact a dense cloud or galaxy and produce noticeable excess emission and morphological changes. A detailed discussion of other evidence for jets striking clouds appears in Higgins, O'Brian & Dunlop (1999).

Canto & Raga (1996) studied two-dimensional (2-D) jets both analytically and numerically; their work was restricted to the special case where the jet's diameter was very small compared to the cloud's size. They found that in this situation the jet is deflected by the cloud without substantially disturbing the bulk of the cloud; in most circumstances, the jet basically drills a hole through the cloud. Other recent 2-D simulations were performed by Steffen et al. (1997) in the context of jets hitting gas clouds in the narrow-line regions of Seyfert galaxies.

Previous three-dimensional (3-D) simulations of the interactions of a jet with a cloud were presented by De Young (1991), who found that jet/cloud interactions could deflect jets only transiently. Furthermore, his models indicated that strong jets would quickly disrupt clouds, while weak jets would be so dramatically slowed that they should disrupt.

This earlier work made the significantly limiting supposition that the jet densities equaled ambient medium densities, while the clouds were 100 to 10,000 times denser than either. Since the grid was relatively coarse, at 40×40×100 zones, the narrow jets he modeled were not transversely resolved in De Young's work; furthermore, the "beam scheme" code (Sanders & Prendergast 1974; De Young 1991) is highly dissipative and did not employ techniques that could optimally resolve shocks and contact discontinuities. Another early 3-D computation by Balsara and Norman using a Riemann solving code was described by Norman (1993). Their higher resolution approach found that a pair of oblique shocks could form in the region where the jet impacts the cloud, effectively yielding a de Laval nozzle which reaccelerates the flow and produces a fairly stable bent jet. This code was not extensively tested or calibrated, and the results differed from those of De Young. Thus the question of the outcome of jet/cloud interactions certainly could benefit from reinvestigation using well tested codes and more powerful computers.

Very recently, and after this work was well underway, Higgins, O'Brian & Dunlop (1999) presented several 3-D adiabatic simulations aimed at studying the effects of different hydrodynamical and geometrical parameters in attempts to reproduce the observed structure of radio sources, particularly WATs. Their code is based on the Godunov method of Falle (1991) and assumes reflection symmetry about a plane bisecting the cloud and the jet. Higgins et al. also estimated the intensity of synchrotron emission for the jet in order to make approximate matches to the observed radio maps with bends or hot spots. de Gouveia Dal Pino (2000), using a 3-D code using the smoothed particle hydrodynamics technique, has just completed a similar series of interaction simulations focussed on conditions expected for the jets emerging from protostellar nebulae which are associated with Herbig-Haro objects. She found the deflected beams looked similar to some observed Herbig-Haro systems. In this case, however, unlike the radio jet situation, the density of the jet is larger than that of the ambient medium, and cooling is important. We would thus expect the bent protostellar jets to be relatively more stable than lighter extragalactic jets, and a comparison with her results should be less illuminating than a comparison with those of Higgins et al. (1999).

In this paper, we expand upon our previous 3-D simulations involving interactions of jets with asymmetric environments (Hooda & Wiita, 1996, 1998; hereafter HW96, HW98) to investigate the situation where a jet impacts a massive cloud in the interstellar medium. The most important parameters for our simulations are the density ratio between the jet and the ISM, the density ratio between the ISM and the cloud, and the jet Mach number. We describe our numerical approach and input parameters in §2. In §3, the results of simulations are given. In §4 our results are discussed and compared with those of other groups. Our conclusions are presented in §5.

2. Numerical Setup and Input Parameters

2.1. Code

These simulations employed the well-tested general purpose three dimensional code ZEUS-3D, v.3.4 (Clarke & Norman 1994; Clarke 1996a), an extension of the two dimensional code ZEUS-2D which is described in depth in Stone & Norman (1992a,b), and Stone, Mihalas, & Norman (1992). This incarnation of ZEUS-3D is an explicit Eulerian finite-difference code employing the piece-wise parabolic advection method (PPA) of Collela & Woodward (1983). Shock waves are treated using the von Neumann-Richtmyer prescription for artificial viscosity. The algorithms used in these codes have been tested extensively against a variety of flow problems where the solution is either known analytically or has been determined experimentally (Stone & Norman 1992a; Clarke 1996a). The code works very well in most situations, but gives small errors for shocks inclined at angles to the grids. Additional details are given in HW96.

Our simulations were carried out on the San Diego Supercomputer Center (SDSC) Cray T90, and postprocessing was performed using Spyglass/Fortner TRANSFORM and NCAR interactive graphical software packages.

2.2. ISM and ICM

For the ambient media through which the jet propagates, we use the same density and pressure structures that were employed in our earlier efforts (HW96, HW98). The ISM is taken to be isothermal with a nominal temperature, $T_{\rm ISM} = 10^7 K$, and density varying as

$$\rho(x, y, z) = \frac{\rho_0}{\{1.0 + [(z/z_{scale})z_H/(z_H - x\tan\theta)]^2\}^b} \tag{1}$$

where $z_H - x\tan\theta$ represents the longitudinal (z) location of tilted interface between the ISM and the ICM and z_H is given in multiple of the initial jet radius, R_0, which defines the length unit for our calculations; z_{scale} is the scale length for the density of an ISM with power-law decline (of half-index b) along the z-direction. To provide physical units, we choose the initial number density $\rho_0 = 0.01$ cm^{-3} at $z = 0$. We set $z_H = 30, z_{scale}$=26.7 and $b = 0.6$ for our all simulations (see HW96 for a discussion of parameter choices). The interface tilt angle from the $x - y$ plane is set as $\theta = 30°$. On crossing the ISM/ICM interface, the density drops to $0.2\rho(z_H)$, while the temperature rises by a factor of 5 to provide a pressure-matched boundary; the density and pressure for the ICM, i.e., for the region, $z > z_H - x\tan\theta$, are kept constant.

These simulations were all run on grids of 250 active uniformly spaced points along the jet propagation direction for $0 \leq z \leq 45$. Eighty active zones are used in both the transverse (x and y) directions, with 36 uniform zones of between $-1.2 \leq (x, y) \leq +1.2$ and 44 ratioed zones from $1.2 \leq |(x, y)| \leq 12$, with the smallest being 0.0667 initial jet radii in size. (See HW96 and HW98 for more details.)

2.3. Jets

In that the morphologies of powerful radio sources strongly support the idea that the jets' densities are substantially less than those of the ambient medium (e.g., Norman et al. 1982) as well as supersonic, we employ jet densities usually set to $10^{-1.5}$ of the initial ambient galactic gas density ($\eta \equiv \rho_j \ / \ \rho_{\rm ISM}(0) = 0.0316$). The initial radius of the jet, R_0, our basic size unit, is set to a canonical value of 1 kpc when we evaluate quantities in physical units but of course everything can be scaled for different assumptions about the jet size. For all of our simulations, we assume that the jet's initial pressure matches that of the ISM at $z = 0$; therefore, for example, the initial nominal temperature of the jet is $T_j = 3.16 \times 10^8 K$ for $\eta = 10^{-1.5}$, supposing that mean molecular weights are the same for the jets and the ambient media. The other important parameter we vary in this work is the jet Mach number $M_j \equiv u/a_j$, where u is the initial jet velocity and a_j is the sound speed in the jet. For the nominal ambient temperature of 10^7K and scale length of 1 kpc, the time unit used in our simulations is $\approx 2.0 \times 10^6$yr. Table 1 identifies our five complete simulations in the first column, and gives the Mach numbers and jet/ISM density ratios used in them in the second and third columns.

2.4. Clouds

In these simulations a cloud is always set up as a symmetric sphere which is denser than the ambient medium surrounding it. The density of the cloud is obviously very important, and in our simulations we took η_{cl}, the ratio of the central density of the cloud to the density of ambient medium, as an input parameter given in Column 4 of Table 1. In all cases we set the radius of the cloud, $R_{cl} = 4.0R_0$. This value is a reasonable size for a giant cloud complex in the interstellar medium or for a small galaxy (perhaps in the process of merging with the active galaxy). Still, this choice of cloud size (radius 4 times that of the jet) was primarily motivated by its improving the opportunity to develop more interesting interaction effects, particularly in comparison to the more easily analyzed cases where the the cloud is much larger than (or smaller than) the jet's diameter.

The cloud's density is taken to vary as a quasi-power-law decline with distance (r_{cl}) from the center of the cloud as

$$\rho(r_{cl}) = \frac{\eta_{cl}\rho(X,Y,Z)}{[1.0 + (r_{cl}/r_{scale})^2]^{b_{cl}}} \tag{2}$$

for $r_{cl} \leq R_{cl}$, and 0 elsewhere. In Eqn. (2) (X, Y, Z) is the location of the cloud's center, and r_{scale} is a scale length for the density decline which basically determines the sharpness of the interface between the cloud and the ISM; b_{cl} is the power-law index within the cloud. The r_{scale} value is chosen as an input parameter for the clouds (column 5 of Table 1), while b_{cl} is then computed by our cloud subroutine so as to make the density of at the edge of cloud smoothly match the average density of ambient medium around the cloud at $r_{cl} = R_{cl}$.

We considered clouds that are either isothermal or isobaric with respect to the surrounding ISM (column 6 of Table 1). Since the density of a cloud declines from the center to the edge, an internal pressure gradient exists in a cloud set up to have a higher density but the same temperature as the surrounding ISM (isothermal case); such a cloud is unstable to expansion on a long enough time scale. However, for fast jets (fairly large Mach numbers) and not terribly overdense clouds, we found the cloud was effectively stable long enough for the interaction with a jet to be completed. Our runs A and B satisfy this criterion and we have utilized isothermal clouds for our most extensive simulations of this type. For runs with slower jets and denser clouds, the time during which the jet and cloud interact is longer, and we set the clouds to the isobaric type; otherwise they would spread out on their own before the jet has finished interacting with them. Such isobaric clouds have temperatures which rise from their cores to their edges.

The cloud is offset in the x direction, which allows the jet to hit it approximately at an 45° angle, thereby maximizing the chance of seeing the jet bending (e.g., Stocke et al. 1985). Explicitly, we have always chosen (-2.0, 0.0, 6.0) to be the coordinates of the cloud center, with the center of the jet's base set at (0,0,0). With this choice of cloud location, the jet hits the cloud rather early in the simulation, thereby allowing the post-interaction development in which we are predominantly interested to consume the bulk of the computational effort.

The geometrical structure of our simulations can be seen in Figure 1. A jet goes in from the center of the grid on the left while the center of a cloud is offset by 2 length units from the axis of the jet. There is a tilted interface between the ISM and ICM visible on the right side of Fig. 1. The transverse zones are small and constant in size close to the jet axis, so that 30 zones span the jet diameter, thereby allowing internal structures to be well resolved. The outer transverse zones are ratioed so as to adequately cover the less important interactions far from the jet axis. The coordinate grid extends to ± 12 in the transverse (x and y) directions, and from 0 to 45 in the longitudinal (or axial — z)

direction, with lengths given in units of R_0, the initial jet radius.

3. Simulation Results

3.1. Powerful Jets

In runs A and B, we explore the interactions between fairly fast jets (M_j of 6 and 3, respectively) and relatively low mass clouds (η_{cl}=10). The density of these clouds are set to change rather rapidly from their centers (r_{scale}=2.0); for clouds with a fixed radius and the same central density, a smaller r_{scale} implies a smaller total cloud mass.

We describe the entire jet/cloud interactions for Runs A and B in terms of four stages. The first stage is when the jet just starts to contact the cloud, as shown in Fig. 1. The jet hits the cloud off-center; this figure also clearly shows the Mach disk terminating the jet and the bow shock propagating into the ambient ISM in front of the jet. The times required to get to stage 1 for our powerful simulations are very short, with $t \approx 0.1$ for Run A and $t \approx 0.2$ for the half-as-fast Run B.

The second stage is defined as beginning when the bow shock arrives at the distance $z = 6.0$, where the center of the cloud is located along the direction of jet propagation. Fig. 2 shows this stage in its upper panels. As can be clearly seen, the bow shock is not symmetric with respect to the jet because of the strong interaction with the cloud; it is shifted upwards, into the less dense part of the ISM. Therefore, a tilted interacting surface is formed along the region of intersection of the bow shock with the cloud. This region and the surrounding area within the cloud are denser because the cloud is being pushed and compressed by the jet. The times when this stage is reached are $t = 0.84$ and $t = 2.08$, respectively, for Run A and Run B, thereby illustrating a relatively greater deceleration for the $M_j = 3.0$ case.

The basic shock structures around the jet are almost the same for Runs A and B; however, the Run B jet produces a broader cocoon than does the faster Run A jet. In the $y - z$ plane, where the cloud is centered and the ISM is not tilted (as is seen in the density image of the central $x = 0$ plane for Run A in Fig. 3, upper-left panel), the bow shock along the z direction in front of the jet is symmetric, and a symmetric cocoon is also seen. Fig. 3 (upper-right panel) also shows the pressure in the $z - x$ central plane for $t = 0.84$ of Run A. The image illustrates the modest tilt in the isodensity and isopressure surfaces in the ISM, a slightly tilted intense interaction area, with the highest pressure between the jet and the cloud in the region where the jet strikes the cloud, as well as a longer sharply defined high-pressure area which corresponds to the compressed and pushed portion of the cloud. We can see this whole "working area" exhibits high pressure and presumably significant synchrotron emissivity. Furthermore, the pressure of the cloud is also higher than that of the ambient medium around it, since we set the cloud up so as to be isothermal with the ISM.

As the jet continues to propagate, the cloud is pushed away and eroded. Fig. 2 also shows this intermediate stage 3 for both of our more powerful jet simulations (middle panels), when the clouds were totally displaced from their original positions by the impact of the jets. The time for Run A to reach this stage is $t = 2.16$, and for Run B, $t = 4.88$; therefore, the total interaction times (which we define as the interval between the beginning of stage 1 to this intermediate stage 3), are $t_{int} = 2.04$ and 4.64, for Run A and B, respectively. Interaction times defined in this way are recorded in the last column of Table 1 for all the simulations. It is obvious that the cocoon is very asymmetric by this point. Most of the interaction remnants flow upwards away from the cloud into the low density ISM, while there is a much smaller cocoon along the lower part of the jet. This side of the cocoon is very thin, especially for Run A, since the cloud has compressed the backflow in the cocoon on the lower part of the jet. Most of the backflow is diverted upwards thanks to the interaction with the cloud, thereby making a broader upper portion of cocoon; for Run A, this 'upper' cocoon is as wide or even wider than the corresponding part of the cocoon in Run B. The internal structures of the jets, exhibiting reconfinement shocks, are clearly shown in Figs. 2 and 3.

We also show the pressure for the Run A case (Fig. 3, lower-left) at the same time as the middle density graph ($t = 2.16$) in Fig. 2. The pressure plot indicates a similar structure to the earlier stages, in the sense that the two regions with the highest pressure are one small spot-like interacting area just in front of the jet, and one larger area which is a part of the pushed cloud. Some of the working area as defined in the density image is found to have a relatively low pressure, while the distorted cloud retains its high pressure.

The last stage we present for these strong jet cases is at the point when the jet crosses the interface between the ISM/ICM after undergoing interaction with the cloud. The two images at the bottom of Fig. 2 are the final stages for the runs, with respective times of $t = 6.4$ for Run A and $t = 17.52$ for Run B. We stopped Run A when the Mach disk of jet finally arrives at $z = 32$; the jet in the Run B was allowed to propagate a little further, and reaches the same place at $t = 15.4$. Thus, the times required to reach the interface are in the ratio 2.4:1.0 for Run B:Run A. Since the initial Mach numbers and velocities were in a direct 1:2 ratio, this quantifies how the jet in Run B is more severely affected and slowed through its interaction with the cloud. Furthermore, the time for the bow shock preceding the jet to reach the interface is $t = 6.04$, which is 1.0 time units longer than the M6 run presented in HW98 (which was cloudless, but otherwise identical to Run A). We thus see that the dalliance with the cloud slowed the progress of the Mach 6 jet by just about 20%.

As is clear from Fig. 2, the slower Run B jet develops a broader cocoon, as expected from earlier simulations (e.g., Norman et al. 1982 in 2-D; HW 96, HW98 in 3-D), and evinces a substantially unstable and wiggly structure by the end of the simulation. Figure 4 gives several cross-sectional slices of both density and z-direction velocity through the Run B jet at $t = 17.52$, further illustrating this point. The jet cross-section changes from circular to more complex, eventually becoming ribbon-like at large distances from the origin. This illustrates the growth of unstable non-axisymmetric modes, dominated by an elliptical shape change and a helical rotation (e.g., Hardee, Clarke & Howell 1995). Regions exhibiting significant backflow form rather close to the jet, and illustrate that the Mach 3 jet is coming close to breaking up at a significantly earlier stage than did the similar simulation (M4) described in HW98.

The faster Run A, on the other hand, takes a much shorter time to reach the interface, and remnants of the high density cloud can still be seen embedded in portions of the bow shock towards the end of the simulation. The Run A jet also shows relatively stable inner structure, though weaker non-axisymmetric modes have clearly been significantly excited by then; the last panel in Fig. 3 indicates the pressure structure for the final stage of Run A. The highest pressure region, corresponding to the radio "hot-spot" is certainly still in front of the main jet; the main interaction region is in one compact area, and is a weakened Mach disk. A longer curved region shows higher pressure than the rest of the compressed ambient medium. The main interaction area, which evinced a spot-like structure at the earlier times, now shows a wiggly morphology, indicating the non-linear growth ofrnon-axisymmetric modes.

In both cases, the rates at which instabilities develop is larger than for identical or very similar simulations performed with no clouds in the way of the jets; those earlier computations were only subjected to very weak non-axisymmetric perturbations due to the tilt of the ISM isobars with respect to the jet normal (HW96, 98). While that tilt did induce minor deviations from axisymmetry, we note (without surprise) that hitting a much denser cloud is far more effective in engendering instabilities. Nonetheless, for these rather fast, light jets, we see that the clouds are quickly destroyed. This is true even for isobaric cloud simulations for otherwise identical parameters that we carried out to check if these results were sensitive to the cloud structure. Although these isobaric simulations were only computed for substantially shorter times, during those interaction periods (roughly up to stage 3) no significant differences were seen in the morphologies of the isobaric and isothermal situations. In particular, the cloud was essentially as stable for the isothermal case as for the isobaric one, which is unsurprising, given the relatively brief interaction times.

3.2. Weak Jets

Run C is a case with a low velocity ($M_j = 1.5$) jet striking a dense cloud ($\eta_{cl} = 50$). The other parameters are given in Table 1. The cloud density scale is changed to 4.0 to make the ISM/cloud interface more abrupt and simultaneously to make the cloud even more massive. To prevent any expansion during the lengthy interaction phase, this (and all subsequent) cloud(s) is(are) set to be of the isobaric type instead of the isothermal situation considered for the complete versions of Runs A and B discussed in §3.1. We show the interaction process in the left portion of Figure 5, which illustrates results only out to an axial extent of $z \leq 24$, so as to give a more detailed image of the interesting portion of the computational grid. The times for the two panels for Run C in Fig. 5 are $t = 4.0$ and $t = 9.44$, respectively. After the jet impacts the cloud, it makes slow headway, and finally is effectively stalled by the cloud. To quantify this point, the distance the jet progresses is only ~ 1.5 spatial units between $t = 4.0$ and $t = 9.44$, despite having traveled $\sim 4.2R_0$ out to $t = 4.0$, and the advance of the jet continues to decelerate throughout this period. The mean head velocity corresponds to about 3% of the jet's input velocity during this interaction.

The interaction between the jet and cloud gradually yields a cocoon with a nearly circular longitudinal cross-section on the side away from the cloud (Fig. 5, top-left). Some significant backflow along the jet is seen to form on the side striking the denser parts of the cloud (Fig. 5, bottom-left). As can be seen in the later stage of evolution in Fig. 5, the main body of jet is actually bent a little bit downwards into the cloud, instead of being "refracted" away from it. This counterintuitive result can be explained in terms of the interaction between the faster forming cocoon on the upper side and the jet itself; the vortical flow in the cocoon exerts pressure on the jet on the side away from the cloud; this tends to push the jet deeper into the dense cloud core. While a narrow, very slow stream of matter is seen to flow upward, along the jet/cloud interface, we note it really just feeds into the the "circular" cocoon. Of course, the cloud is being affected by the jet's impact upon it and is significantly distorted by the bow shock. By $t = 9.44$ the cloud has lost its spherical shape, but could clearly resist the onslaught of this feeble jet for a much longer time. Thus, we argue that this very weak jet is effectively destroyed by this very dense cloud.

In order to investigate a more intermediate case of jet power against cloud resistance, we increased the Mach number of the jet to 2 and decreased the central density of the cloud to 25 in Run D; all other parameters are the same as for Run C. The results for $t = 4.0$ and 10.08 are also shown in Fig. 5 (right side). Compared with Run C at $t = 4.0$, the jet of course has moved more deeply into the cloud and makes a broader cocoon. A tilted interaction area forms in the front of the jet. Nonetheless, the vortical backflow exerts pressure on the jet from the top side, thus causing the penetrating part of the jet to bend slightly downwards.

As time goes along, the jet keeps advancing less and less rapidly, but it does manage to push the cloud slowly outwards. By $t = 10.08$, shortly before we terminated this simulation at $t = 11.76$ (Fig. 5), the jet has almost gone through the entire cloud and has eroded most of the top half of the cloud, reaching a maximum distance of $z = 9.1$. A very extensive cocoon forms on the top side of the jet. The interaction between the cocoon and induces the jet to evince a substantially wiggly structure. Again, there is a curved interaction area where the jet hits the cloud, which squeezes a weak stream of plasma upward. This stream gains a vortical motion near the uppermost portion of the cloud as it merges into the circular cocoon. Fig. 5 also illustrates how a weakend bow shock has propagated far ahead of the stalled jet; it extends a little bit further on the upper side. Given the extremely slow rate of progress, despite substantial computational cycles being required, we did not follow this simulation further. Considering the results from Run B, we are certain that the jet would soon become quite unstable. We note that this type of weak transonic flow provides a good model for many Fanaroff-Riley Type I sources (e.g., De Young 1991; Bicknell 1995; Gopal-Krishna & Wiita 1999).

3.3. A Bent Jet

The final simulation we present, Run E, is of a relatively slow, but rather heavy, jet. In this simulation, we raise the density of the jet so that $\eta_j = 0.316$, ten times the value of the jet's density in Runs A–D; all other parameters are set to the same values as in Run C. However, since the pressure of the jet is always chosen to be equal to the pressure of ambient medium at the inlet, this increase in density implies a drop in jet temperature, so the absolute velocity of the jet is indeed decreased by a factor of $(1/10)^{1/2}$, even though we set $M_j = 1.5$, the same as for Run C.

The results of the Run E simulation are shown in Fig. 6, which again shows results only out to an axial extent of $z \leq 24$. At first, when the jet just starts to interact with the cloud, the morphology is very similar to those of Run C or Run D (§3.2), with a broader cocoon extending beyond the jet being formed by the upwards stream, while a thin cocoon forms below the jet (upper left panel of Fig. 6, corresponding to $t = 8.0$). However, after a short time of interaction, a quite different structure forms. As can been seen from the right top panel of Fig. 6 ($t = 11.2$), a small tail-like shape forms below the jet while a cocoon with a quasi-circular cross-section forms on the top of the jet. However, in this case the material feeding the cocoon is in the form of a definite beam emanating from the locale where the jet impinges upon the cloud; this beam extends upwards along the cloud.

This Run E basically retains this structure for a very extended time as the maximum extent of the main jet slowly advances with nearly constant velocity; therefore we could reasonably estimate the total interaction time quoted in Table 1 as $t_{int} = 20$, even though we did not follow the simulation out quite that long. At the same time, the lower "tail" continues to extend downwards and backwards, while the upward beam interacts with the upper portion of the cloud and the ambient ISM. A very broad cocoon forms above the incident jet, and behind the bent beam. This bent beam extends for a distance substantially longer than the diameter of the jet, and by the time we end this simulation, it has extended nearly as far as the original jet traveled before it struck the cloud (cf. bottom-left panel of Fig. 6, for $t = 17.6$). This panel also shows that the small tail eventually breaks up near its middle. The whole tail and the bent beam are nearly collinear, forming an extended structure, which extends beyond the position of the original cloud, at a nearly 45° angle to the jet direction.

The pressure image at $t = 17.6$ is shown in the bottom-right panel of Fig. 6. The standard reconfinement shock is clearly seen in the main jet before it strikes the cloud. In the high pressure region of the interaction area between jet and cloud, we can see a weak double shock structure that manages to divert much of the matter in the original jet upwards. This structure is very similar to one obtained by Balsara and Norman (Norman 1993). We note another high pressure region along the area where the bent beam strikes the ambient medium and upper part of the cloud. Although these calculations contain no magnetic fields, the increase in both density and pressure would imply this corresponds to a weak hot spot; however, the highest pressure remains at the location where the original jet collides with the cloud, so the most intense synchrotron emission is still expected to arise there. The pressure map also clearly shows how a weakened bow shock has now propagated far beyond the cloud.

4. Discussion

Using the well-tested Zeus hydrocode, we have performed and analyzed a series of 5 simulations for jet/cloud interactions, which we believe adequately span the interesting range. Our parameters also come close to covering the range considered some time ago by De Young (1991), who used a very dissipative code and lower resolution, as well as computations made at more similar resolutions by Balsara and Norman (Norman 1993) and Higgins et al. (1999); while these last two groups used significantly different types of codes (cf. §1), they should be generally comparable to ZEUS in accuracy.

Still, there are several significant differences between the approach we have taken and those of earlier efforts to address the effects of jets striking clouds. We set the density of the cloud declining with truncated power-laws from center to edge of the cloud, which we believe is somewhat more realistic than the hard-edged clouds assumed by the other authors; this is more particularly true if the "cloud" is really the gas associated with a smaller galaxy in the process of merging with the larger active galaxy. Also, some important parameter choices are significantly different. For example, in De Young's simulations, the density of the jet is set to be equal to the density of ambient medium (which was assumed to be of constant density, aside from any clouds), and the velocities of all cases were the same; as noted in many earlier simulations (e.g., Norman et al. 1982), most jet morphologies are only well explained if $\eta \ll 1$, so our values of η are more reasonable than those of De Young (1991). Higgins et al. (1999) chose density ratios of jet to ambient medium and cloud to ambient medium similar to ours, but, because the fiducial temperature they assumed for their jet was higher than ours, the absolute velocities of their jets are larger than those we considered, even for similar Mach numbers. For this reason, runs with the same Mach numbers in their work would require denser clouds to produce similar effects. Nonetheless, we and the other authors have certainly investigated similar jet/cloud cases: a light, fast jet striking a moderately massive cloud; a light jet hitting a more massive cloud; a heavier, slow jet impacting a massive cloud. Thus, it is clearly worthwhile to compare our results with theirs.

For the case of fast jets and less massive clouds our Runs A and B, Case I-1 of De Young (1991) and simulations 3 and 4 of Higgins et al. (1999), all show that the less massive cloud can be pushed away and finally destroyed. However, the parameters we chose did not give rise to the temporary bent jet argued for by the other authors. In the short interaction time relevant for these fast jets, our code yielded only non-symmetric cocoons around the jet. In other words, striking the cloud off-center forced most of the back-flow towards the side away from the cloud. Recall that for De Young's simulations, the density of jet is set to be equal to the density the ISM, which will clearly cause differences in results even the ratios of the cloud density to jet density are similar. In particular, his jet thereby has an effectively higher thrust, and therefore more coherence, possibly explaining the bulk of the differences; in addition, his jet is not well resolved transversely, so the effects of internal shocks could not be incorporated in his efforts. We were somewhat surprised to see that there are bends seen early in the simulations of Higgins et al., particularly since we note the absolute velocities of their jets are very large for their fastest jets (~ 0.36c), which is over six times larger than velocities (~ 0.057c) of our fastest jets. This difference comes about because their canonical values are $\eta = 0.01$ and $T_{ISM} = 5 \times 10^7$K compared to the $\eta = 0.0316$ and $T_{ISM} = 1 \times 10^7$K for most of our simulations. As the bends they found are rather short-lived, this difference in results is probably not too important, and might be related to their assumption of reflection symmetry, which we do not employ.

Our Run C, the case with a slow and weak jet but dense cloud, is somewhat similar to the Case I-2 in De Young's simulations (except that he always chose $\eta = 1$, and larger values of η_{cl}) and more similar to Simulations 1 and 2 in Higgins et al.'s work. De Young states that the weak jet is first bent nearly 90 degrees, but that the jet will eventually erode the cloud. We do find a similar small bent stream which apparently corresponds to the trajectory of marker particles in De Young's work; however, we would not classify this flow as a continuing jet, given its small radius and associated weak thrust. No strong deflection, shown in Simulations 1 and 2 of Higgins et al., has been found in our Run C; instead, the weak upwards stream is blocked by the cloud and ambient medium, thus finally forming a cocoon with a circular cross-section on the top side of the jet. Furthermore, our intermediate power Run D shows a jet can go through the cloud slowly, while making a similar, but wider, structure as compared to Run C.

Higgins et al. (1999) performed simulations 5 and 6 for slow, heavy jets, which are similar to our Run E simulation. Our simulation E is also in the general parameter range for the successfully bent jet considered by Balsara & Norman ($M_j = 4, \eta = 0.2$). We find a bent "arm" structure during the process of the interaction with an upward flow, and a downward flowing stream, as did Higgins et al. However, our downside tail is much sharper while the top-side cocoon shows a nearly circular cross-section. Moreover, our pressure image clearly shows the bent stream interacts with the cloud and ambient medium at an area above the jet, and we believe the area could be thought of as another hot spot, which Higgins et al. (1999) have not clearly found in either of their slow, heavy jet simulations. Our modestly better resolution near the jet axis or the reflection symmetry assumed by Higgins et al. could explain this difference, though it could also be caused by the modest differences in the parameters we employed.

5. Conclusions

These simulations have confirmed that certain radio source morphologies can indeed be understood in terms of collisions of jets with massive clouds. Some WAT sources could certainly be produced in this manner, even if most of them can be explained in terms of "stormy weather" induced in the ICM by galactic mergers (e.g., Loken et al. 1995). The small group of "dog-leg" quasars (e.g., 3C 270.1, 3C 275.1, 4C 25.01; Stocke, Burns & Christiansen 1985) are indeed probably best understood in terms of fairly long-lived stages of jet/cloud or jet/small galaxy interactions.

The results of this paper, along with those of De Young (1991), Norman (1993) and and Higgins et al. (1999) strongly suggest that only a small range of parameter space is capable of producing fairly long-lived bent jets. These jets should be relatively dense with respect to the ISM and also relatively slow, as indicated by the lack of such structures in fast, but heavy jet simulations (Higgins et al.'s cases 7 and 8). Alternatively, if the jets started off relativistically, they should have entrained enough matter so as to have become fairly dense and only transonic (e.g., Bicknell 1995), by the time they hit the cloud. Given that only a small fraction of radio sources show morphologies that clearly indicate abruptly bent stable jets, or show associated optical or X-ray emission that allow us to confidently infer an interaction with a massive cloud, the fact that numerical simulations rarely yield such morphologies is not surprising.

Compact Steep Spectrum (CSS) radio galaxies are almost certainly quite young (e.g., Fanti et al. 1990). Nonetheless, there is strong theoretical (e.g., Gopal-Krishna & Wiita 1991; Jeyakumar et al. 1999) and statistical (Saikia et al. 1995, 1999) evidence that they interact with denser and more asymmetric media in the inner portions of their host galaxies than do typical powerful radio galaxies. Carvalho (1998) has performed analytical estimates of how much extra confinement can be accomplished if the medium contains many dense clouds, and he argues that a good understanding of Gigahertz Peaked Spectra and CSS sources can be achieved if jet/cloud collisions are more common in these sources.

More powerful jets will be only slightly and temporarily diverted by interactions with clouds, which they will either drill through (if the cloud is much bigger than the jet's diameter) or demolish (if the cloud is comparable in size to the jet). While we have seen that such jets are rendered more unstable by a collision with a cloud, they would not typically produce morphologies that show clear evidence of the jet/cloud interaction, particularly if the source is viewed at a late stage in its life, by which time the jet has gone wildly unstable.

Finally, very weak jets can be halted (or at least nearly completely confined for very extended periods) when they hit a massive cloud with more than an glancing blow. This type of situation appears to be not uncommon in active spiral galaxies. While Seyfert galaxies rarely show large-scale jets, careful studies of nearby objects sometimes reveal evidence of sub-galactic scale radio jets interacting with gas clouds (e.g., NGC 1068, NGC 4151; Wilson & Ulvestad 1982). These numerical simulations support the idea that weaker jets can indeed be smothered by the more common dense clouds found in spiral galaxy ISMs.

More sophisticated 3-D computations that incorporate dynamically important magnetic fields in a self-consistent fashion (e.g., Clarke 1996b) and also utilize more realistic models for particle acceleration and synchrotron radiation (e.g., Jones, Tregillis & Ryu 1999; Tregillis, Jones & Ryu 1999) will be needed to make models sufficiently detailed so that one could provide convincing explanations of individual sources. While difficult, such simulations are now becoming computationally possible, and they are well worth attempting.

We thank James Joyce and Lynne McKee for producing animations which were very helpful in our analyses of these simulations. This work was supported in part by NASA ATP grant NAG 5-3098 and by Research Program Enhancement funds at Georgia State University. The computations were performed at the NPACI Cray T90 at the San Diego Supercomputing Center under award GSU200.

REFERENCES

Best, P. N., Longair, M. S., & Röttgering, H. J. A. 1997, MNRAS, 286, 785

Best, P. N., Carilli, C. L., Garrington, S. T., Longair, M. S., & Röttgering, H. J. A. 1998, MNRAS, 299, 357

Bicknell, G. V. 1995, ApJ, 101, 29

Canto, J. & Raga, A. C. 1996, MNRAS, 280, 559

Carvalho, J. C. 1998, A&A, 329, 845

Chambers, K. C., Miley, G. K., & van Breugel, W. J. M. 1987, /nat, 329, 624

Clarke, D. A., 1996a, ApJ, 457, 291

Clarke, D. A., 1996b, in Energy Transport in Radio Galaxies and Quasars, ASP Conf. Ser. 100, eds. P.E. Hardee, A.H. Bridle, J.A. Zensus (San Francisco: ASP), 311

Clarke, D.A., & Norman, M.L. 1994, LCA Preprint # 7 (University of Illinois, Urbana–Champaign)

Collela, P., & Woodward, P. R. 1983, J. Comp. Phys., 54, 174

de Gouveia Dal Pino, E. M. 2000, ApJ, in press

De Young, D. S. 1991, ApJ, 371, 69

Fanti, R., Fanti C., Schilizzi R. T., Spencer R. E., Nan Rendong et al. 1990, A&A, 231, 333

Falle, S. A. G. E. 1991, MNRAS, 250, 581

Gopal-Krishna & Wiita, P. J. 1991, ApJ, 373, 325

Gopal-Krishna & Wiita, P. J. 1999, in Lifecycles of Radio Galaxies, eds. J. Biretta, & P. J. Leahy, New Astronomy Reviews, in press

Hardee, P. E., Clarke, D. A., & Howell, D. A. 1995, ApJ, 441, 644

Harris, D. E., Leighly, K. M., & Leahy, J. P. 1998, ApJ, 499, L149

Higgins, S. W., O'Brien, T. J., & Dunlop J. S. 1999, MNRAS, in press; astro-ph/9904009

Hintzen, P., Ulvestad, J., & Owen, F. N. 1983, AJ, 88, 709

Hooda, J. S., & Wiita, P. J. 1996, ApJ, 470, 211

Hooda, J. S., & Wiita, P. J. 1998, ApJ, 493, 81

Jeyakumar, S., Wiita, P. J., Saikia, D. J., & Hooda, J. S. 1999, in preparation

Jones, T. W., Tregillis, I. L., & Ryu, D. 1999, in Lifecycles of Radio Galaxies, eds. J. Biretta & J.P. Leahy, New Astronomy Reviews, in press

Lacy, M., Rawlings, S., Blundell, K. M., & Ridgway, S. E. 1998, MNRAS, 298, 966

Loken, C., Roettiger, K., Burns, J. O., & Norman, M. 1995, ApJ, 445, 80

McCarthy, P. J., van Breugel, W. J. M., Spinrad, H., & Djorgovski, S. 1987, ApJ, 321, L29

Norman, M. L. 1993, in Astrophysical Jets, STScI Symp. Ser. Vol. 6, eds. D. Burgarella, M. Livio, C. O'Dea (Cambridge: CUP), 211

Norman, M. L., Smarr, L. L., Winkler, K.-H. A., & Smith, M. D. 1982, A&A, 113, 285

O'Dea, C. P. ApJ, 295, 80

O'Donoghue, A. A., Eilek, J., & Owen, F. N. 1993, ApJ, 408, 428

Saikia, D. J., Jeyakumar, S., Thomasson, P., & Salter, C. J. 1999, in preparation for A&A

Saikia, D. J., Jeyakumar, S., Wiita, P. J., Sanghera, H. S., & Spencer, R. E. 1995, MNRAS, 276, 1215

Sanders, R. H., & Prendergast, K. H. 1974, ApJ, 188, 489

Steffen, W. S., Gómez, J. L., Raga, A. C., & Williams, R. J. R. 1997, ApJ, 491, L73

Stocke, J. T., Burns, J. O., & Christiansen, W. A. 1985, ApJ, 299, 799

Stone, J. M., & Norman, M. L., 1992a, ApJS, 80, 753

Stone, J. M., & Norman, M. L., 1992b, ApJS, 80, 791

Stone, J. M, Mihalas, D., & Norman, M. L. 1992, ApJS, 80, 819

Tregillis, I. L., Jones, T. W., & Ryu, D. 1999, in Lifecycles of Radio Galaxies, eds. J. Biretta & J.P. Leahy, New Astronomy Reviews, in press

Wilson, A. S., & Ulvestad, J. S. 1982, ApJ, 263, 576

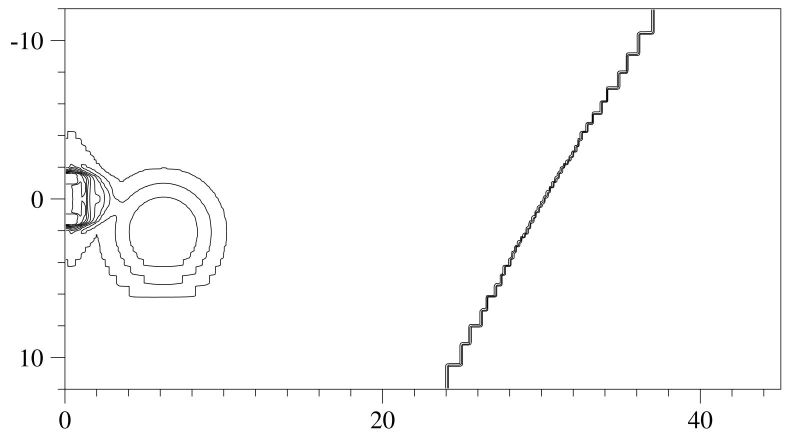

Fig. 1.— Contour graph of $\log(\rho)$ for stage 1 of Run A, with $M_j = 6.0, \eta_j = 0.0316$, and $\eta_{cl} = 10$. This figure, a slice through the entire $z - x$ plane ($0 \leq z \leq 45, -12 \leq x \leq +12$), also shows the general geometry we used in the simulations.

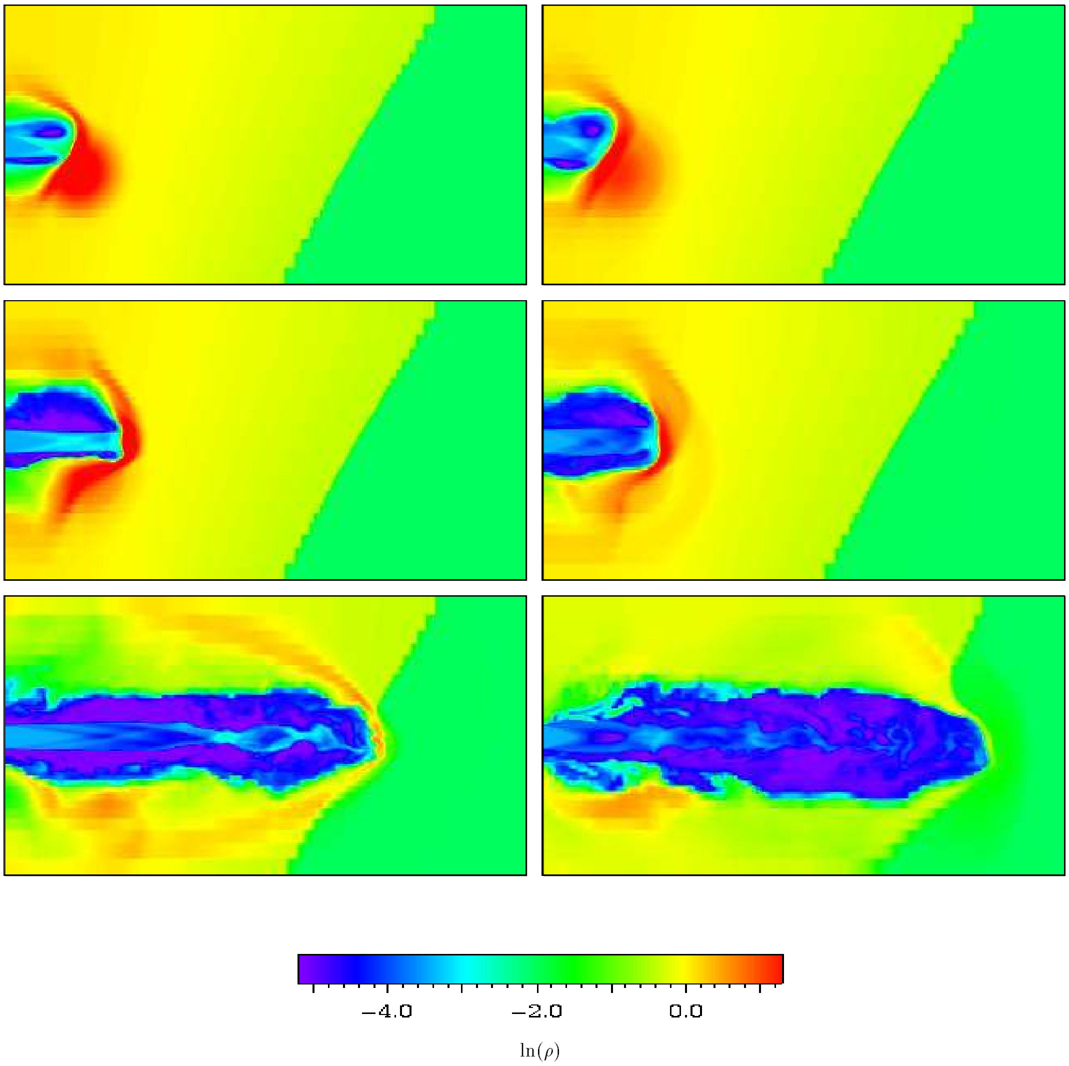

Fig. 2.— The left panels give gray-scale logarithmic density plots for Run A, and the right panels give the same plots for Run B (identical, except that $M_j = 3.0$). These images are in $z - x$ plane slices for $y = 0$ and cover the entire grid. The images for Run A, from top to bottom, correspond to $t = 0.84, 2.16$ and 6.4. The images for Run B similarly correspond to $t = 2.08, 4.88$ and 17.52, respectively.

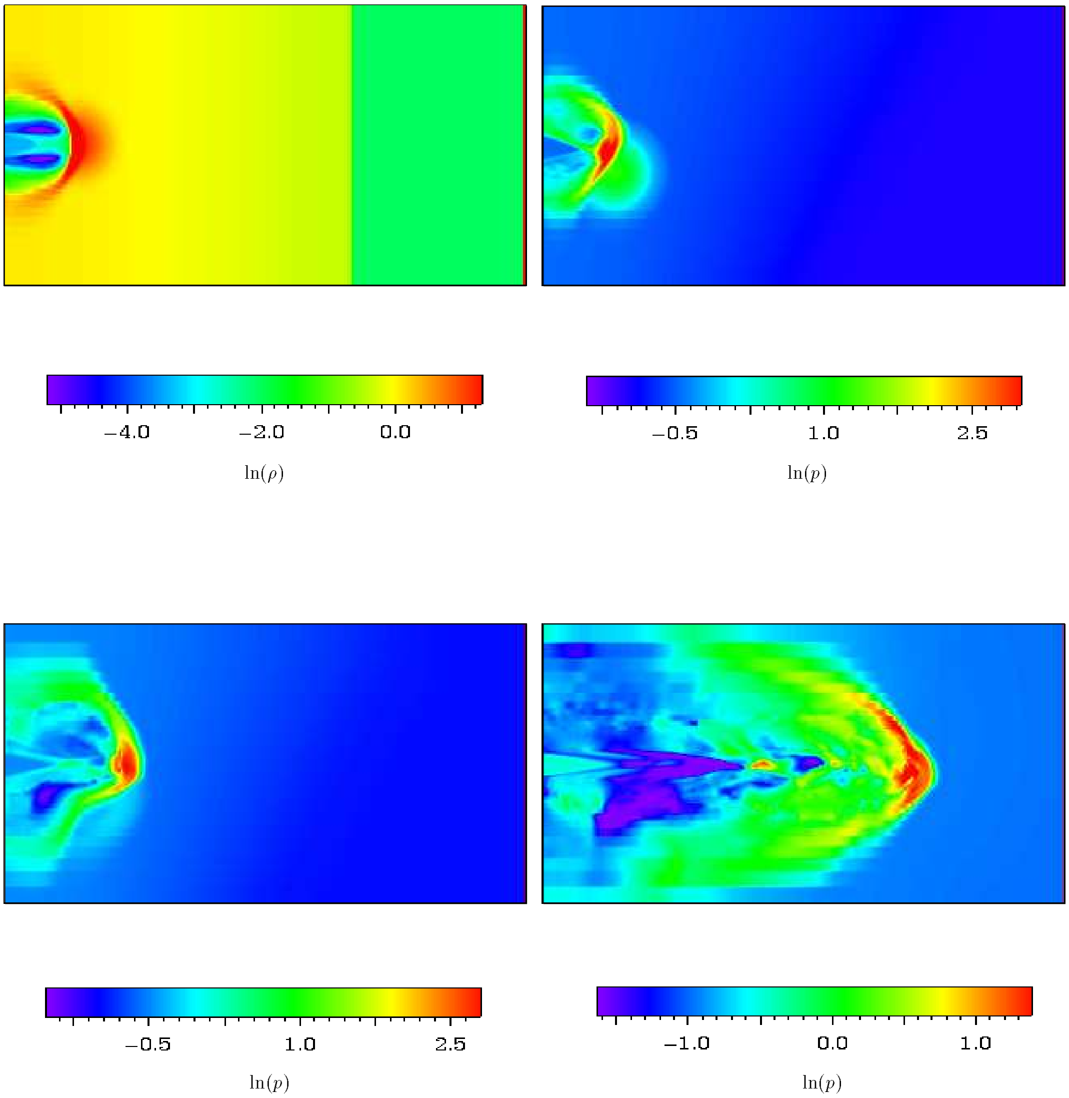

Fig. 3.— The upper portion gives images of Run A at $t = 0.84$. The left panel is the slice of $\ln(\rho)$ in the $z - y$ plane for $x = 0$, and the right panel is the slice of $\ln(p)$ in the $z - x$ plane for $y = 0$. The bottom images give $\ln(p)$ structures of Run A at $t = 2.16$ and $t = 6.4$ in the $z - x$ plane for $y = 0$.

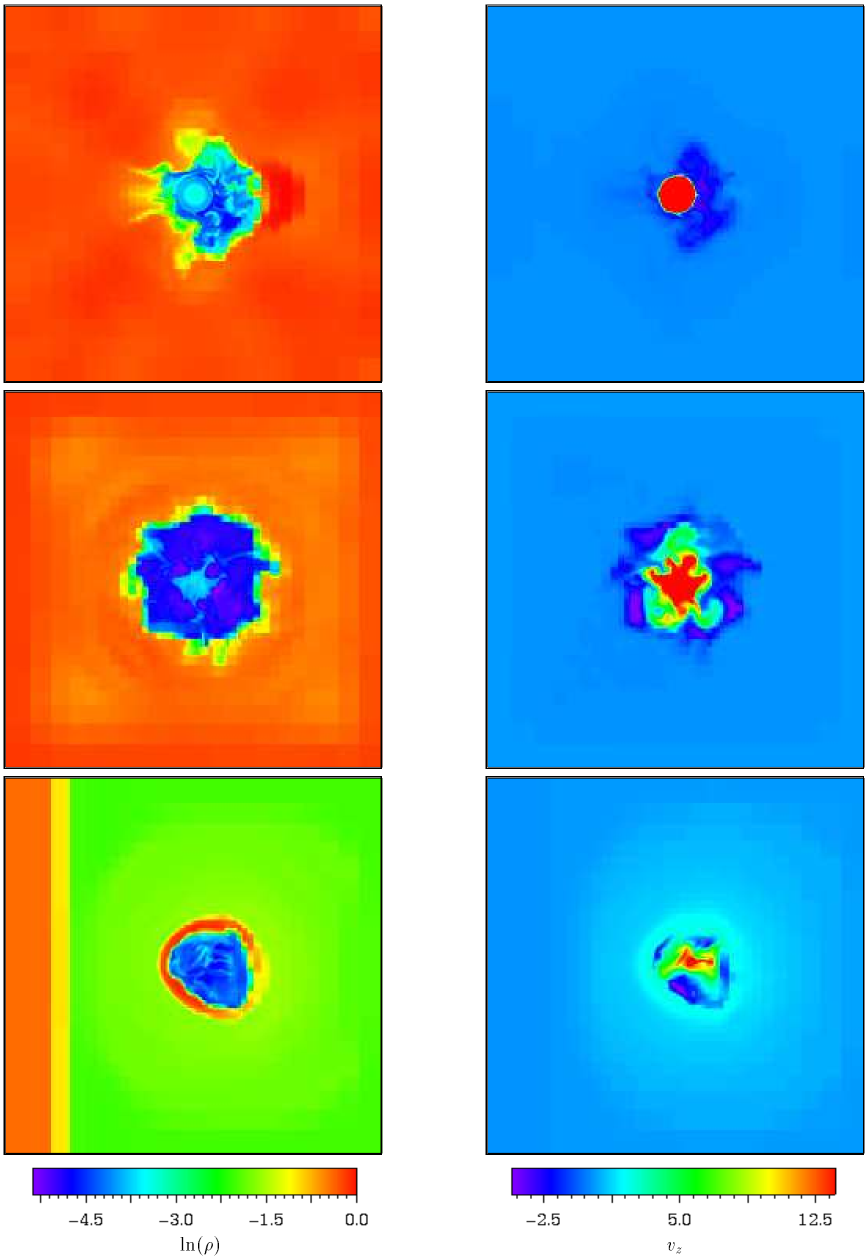

Fig. 4.— Slices of $\ln(\rho)$ (left) and v_z (right) for Run B ($M_j = 3.0$), taken perpendicular to the jet at $t = 17.52$. These slices are located at $z = 1.8, 18.0$, and 36.9, from top to bottom, and illustrate the growth of non-axisymmetric modes.

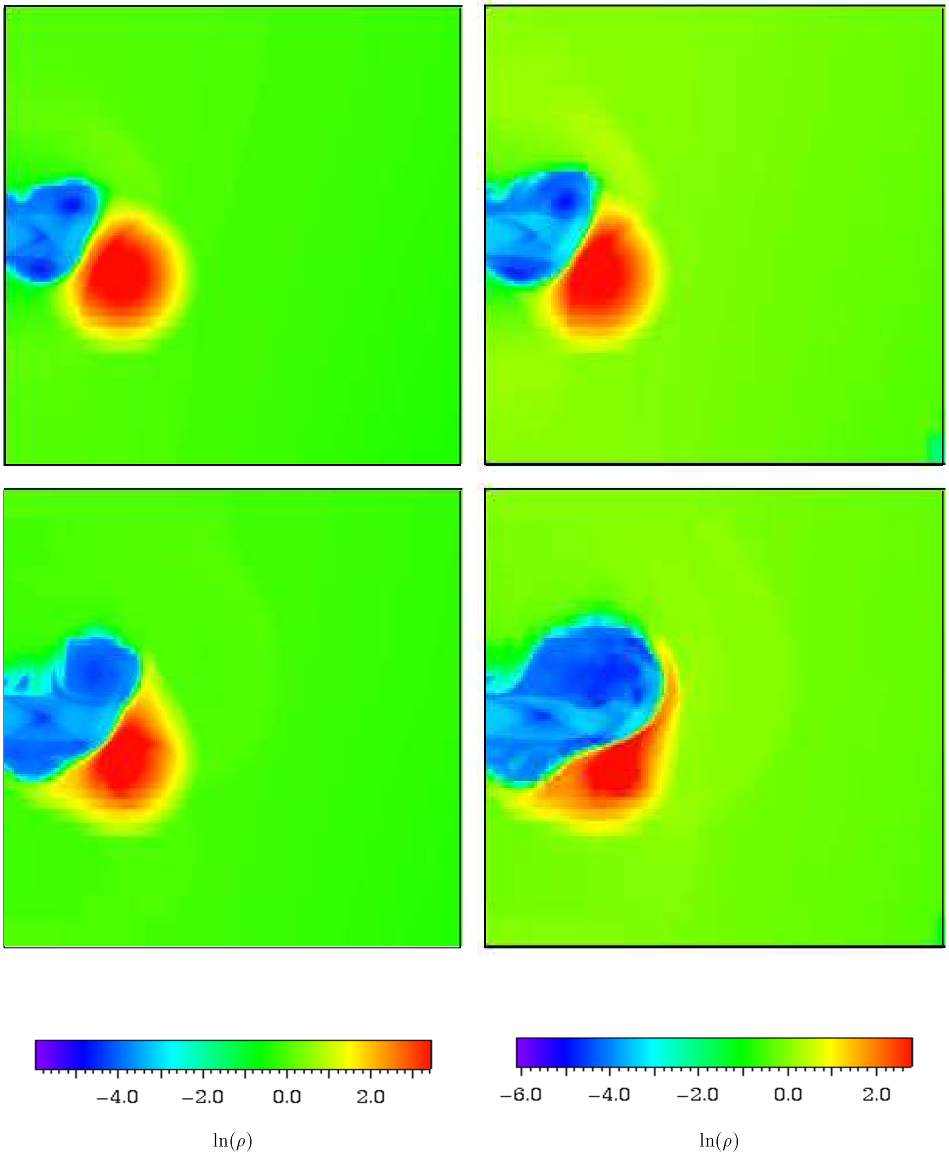

Fig. 5.— The left two panels give images of ln(ρ) for Run C ($M_j = 1.5, \eta_{cl} = 50$) and the right two panels are ln(ρ) images for Run D ($M_j = 2.0, \eta_{cl} = 25$). The times of figures for Run C are $t = 4.0$ and 9.44. The times of figures for Run D are $t = 4.0$ and 10.08.

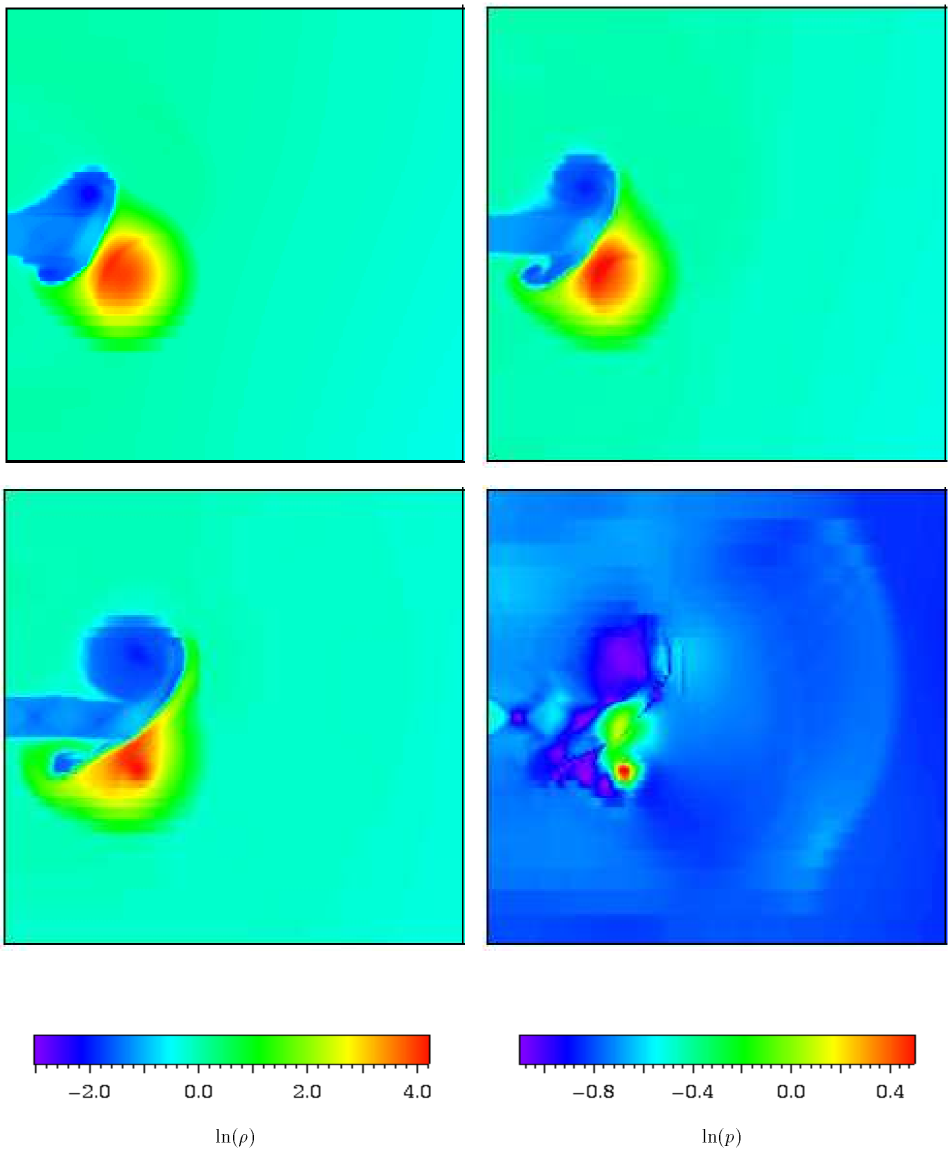

Fig. 6.— The upper and lower-left panels are $\ln(\rho)$ images for Run E ($M_j = 1.5, \eta_j = 0.316, \eta_{cl} = 50$), at $t = 8.0, 11.2$ and 17.6 respectively. The lower-right panel is a $\ln(p)$ image at $t = 17.6$.

Table 1. Simulation Parameters and Interaction Times

Run	M_j	η	η_{cl}	r_{scale}	Cloud type	t_{int}
A	6.0	0.0316	10	2.0	isothermal	2.04
B	3.0	0.0316	10	2.0	isothermal	4.64
C	1.5	0.0316	50	4.0	isobaric	stalled
D	2.0	0.0316	25	4.0	isobaric	11.12
E	1.5	0.316	50	4.0	isobaric	20[a]

[a]estimated, see text for details